Synthesis and Structure Characterization of Ternary Zn_2GeO_4 Nanowires by Chemical Vapor Transport

Chaoyi Yan and Pooi See Lee*

School of Materials Science and Engineering, Nanyang Technological University, Singapore 639798, Singapore

Received: April 15, 2009; Revised Manuscript Received: July 1, 2009

Ternary Zn_2GeO_4 nanowires and their branched structures were successfully synthesized by a chemical vapor transport method. The nanowires showed a rhombohedral crystal phase with dominant growth direction along [110]. The branches exhibited preferential growth directions, which are perpendicular to the backbone due to homoepitaxial growth. The nanowire growth process was explained using vapor−liquid−solid mechanism with Au as catalysts. The present catalytic growth method may offer better control of the morphologies and structures of the Zn_2GeO_4 nanowires, promoting further study of their properties and applications.

1. Introduction

Self-assembled one-dimensional (1D) nanostructures have gained a tremendous amount of attention as promising low-dimensional materials for a wide range of applications in nanoelectronics and optoelectronics.[1−3] Among them, functional oxide nanowires are of special interest because of their unique chemical, electronic, and optical properties.[1,4] A large variety of oxide nanowires have been synthesized, such as ZnO,[1] In_2O_3,[5] Ga_2O_3,[6] SnO_2,[7] GeO_2,[8] MgO,[9] and V_2O_5.[10] Compared with the extensive research on binary oxide materials, investigations on ternary oxide nanowires are relatively limited. However, in most cases, complex ternary oxide materials are technologically important because their properties and hence functionalities can be efficiently tuned by adjusting the ratio of doping or alloying components. In recent years, 1D nanomaterials of several ternary oxides have been successfully synthesized, especially for those ZnO-based ternary compounds.[11]

Zn_2GeO_4, a ternary oxide with a wide bandgap of 4.68 eV, has attracted great attentions for various applications due to its interesting optical properties. Zn_2GeO_4 doped with Mn is known to emit green light,[12] while undoped Zn_2GeO_4 is a native defect phosphor exhibiting white luminescence under UV excitation.[13] Thin-film electroluminescent (TFEL) devices using Zn_2GeO_4 as an active layer have been developed for potential display applications.[12,14] Zn_2GeO_4 was also shown to be a stable photocatalyst for decomposition of water or organic pollutants.[15,16] However, 1D ternary Zn_2GeO_4 nanostructures have rarely been investigated until now. Tsai et al. reported the growth of Zn_2GeO_4 nanorods by aging Zn-containing Ge nanoparticles in water.[17] Huang et al. reported the synthesis of Zn_2GeO_4 nanorods by a surfactant-assisted hydrothermal method.[16] Given the potential research interests that may arise with the unique ternary Zn_2GeO_4 nanowires, exploration of other synthesis methods that yield high quality nanowires is critical for further studies. All previous methods were solution-involved and several drawbacks of the products, such as small aspect ratios,[16,17] low yield,[17] and severely agglomerated morphologies,[16] may inhibit further studies of their properties and applications. Chemical vapor deposition is an ideal synthesis method to produce nanowires with smooth surface, controllable morphology, structure, composition, etc.

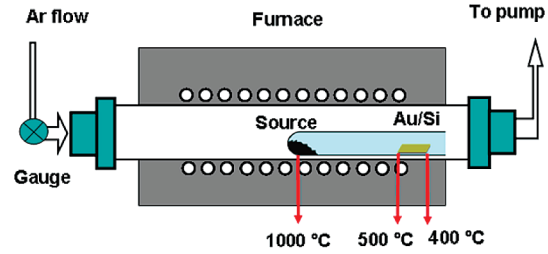

Figure 1. Schematic illustration of the experimental setup for Zn_2GeO_4 nanowire synthesis by chemical vapor transport.

In this paper, we present the successful synthesis of Zn_2GeO_4 nanowires by chemical vapor transport method. High quality Zn_2GeO_4 nanowires and their branched nanostructures were synthesized via vapor−liquid−solid (VLS) process using Au as metal catalysts. Detailed morphology, structure, and composition analyses of the Zn_2GeO_4 nanowires are presented. The metal-catalyzed growth via a chemical vapor transport method may offer significantly better control of the nanowire morphologies and structures, enriching their applications in catalysis and optoelectronic nanodevices.

2. Experimental Section

The Zn_2GeO_4 nanowires were synthesized using a horizontal double-tube system. A schematic illustration of the experimental setup is shown in Figure 1. A small quartz tube (inner diameter 1.5 cm, length 30 cm) with one end sealed was used for chemical reactions and nanowire growth. Mixed ZnO, Ge, and carbon powder (~0.5 g, molar ratio of 2:1:2) was placed at the sealed end of the small quartz tube. Si (100) substrate (width 1 cm, length 1.5 cm) was placed at the open end of the small quartz tube for product collection. Thin Au film (9 nm) was predeposited onto the Si surface using a simple thermal evaporator. The small quartz tube containing source powders and Si substrate was loaded into the furnace chamber, with powder placed at the high temperature region. Central temperature of the furnace was increased to 1000 °C at a rate of 15 °C min^{-1} and kept for 60 min under a constant Ar flow of 200 sccm (standard cubic centimeter per minute). The vapor pressure during growth was 1.9 mbar. The temperature of the source

* Corresponding author. E-mail: pslee@ntu.edu.sg. Phone: (65)-67906661. Fax: (65)-67909081.

10.1021/jp9050879 CCC: $40.75
Published on Web 07/15/2009

powder was 1000 °C during growth. The Si substrate was located in the temperature region of 500−400 °C (Figure 1). Different temperature regions have been tested for the nanowire growth through a series of experiments, and this was determined to be the optimum temperature region with the best nanowire growth in terms of yield and purity. After growth, the furnace was allowed to cool naturally to room temperature.

Morphologies of the products were characterized using field emission scanning electron microscopy (FE-SEM, JEOL 6340F), operating at 5 kV. X-ray diffraction (XRD) data were collected using Rigaku with Cu Kα radiation ($\lambda = 1.5418$ Å) (voltage 40 kV and current 40 mA). Detailed structure analyses were performed in transmission electron microscopy (TEM, JEOL 2010) operating at 200 kV. The chemical compositions were analyzed using energy dispersive spectroscopy (EDS) attached to the TEM. For TEM and EDS analyses, the products were dispersed in ethanol by ultrasonication for 5 min, and then the solutions were dropped on a copper grid coated with holey carbon film. The samples were dried naturally in air before analyses.

3. Results and Discussion

Compared with elemental or binary nanomaterials, synthesis of ternary nanomaterials with stoichiometric compositions is more complex and challenging. Previously, precursor powders were placed at the different temperature zones to enable the simultaneous vapor supply and growth of nanowires with desired composition.[18,19] However, in our case where Ge and ZnO were used as source materials, we suggest that the coevaporation at 1000 °C is essential to ensure sufficient Ge and Zn vapor supplies for the growth of Zn_2GeO_4 nanowires (Figure 1). First, the melting point of bulk Ge is 937 °C. On the basis of our experiments of Ge nanowire growth (Ge powder as source material), sufficient Ge vapor supply and hence a moderate nanowire growth rate can only be obtained when the source powder was heated up to 950−1000 °C. The vapor pressure was significantly lower when lower heating temperature was used (e.g., 900 °C) because the Ge powders were still in solid state (no melting observed after growth). Second, mixed ZnO and carbon powder was one of the most common source materials for ZnO nanowire growth in vapor phase. Previous reports showed that heating temperatures above 900 °C were essential to generate sufficient Zn vapor through carbon-thermal reactions.[20,21] Thus, a heating temperature of 1000 °C was used to generate Ge (through direct evaporation of Ge powder) and Zn (through carbon-thermal reduction of ZnO) vapors for nanowire growth in our experiment (Figure 1).

Morphologies and crystal structures of the products were first characterized using FE-SEM and XRD. Figure 2a is a typical top-view FE-SEM image of the nanowires. Large quantities of nanowires with a high density were successfully grown on the substrate. Enlarged view of the nanowires is shown in Figure 2b. Metal catalyst particles can be clearly observed at the growth fronts of the nanowires (indicated by arrows). Figure 2c is a representative cross-section view of the as-grown nanowires. The diameters of the nanowires are in the range of 10−80 nm with lengths of tens of micrometers. Diameter of the catalyst particle is slightly larger than that of the nanowire stem (Figure 2b, see also Figure 3b). The crystal structure of the nanowires was analyzed using XRD, and a typical diffraction pattern is shown in Figure 2d. The pattern can be readily indexed to Zn_2GeO_4 phase with a rhombohedral crystal structure (JCPDS card 11-0687: $a = 14.231$ Å, $c = 9.53$ Å). No other impurities such as Ge, ZnO, or GeO_2 were detected. The XRD result

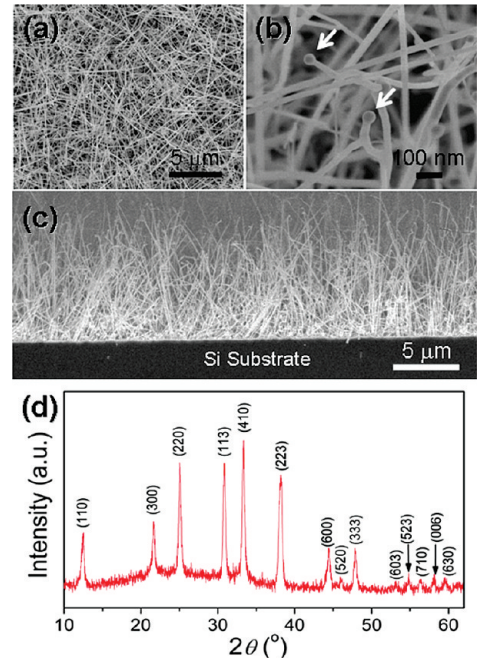

Figure 2. (a,b) Top view FE-SEM images of the Zn_2GeO_4 nanowires at low (a) and high (b) magnifications. (c) Cross-sectional view of the dense Zn_2GeO_4 nanowires grown on Si substrate. (d) XRD pattern showing the rhombohedral phase of the nanowires.

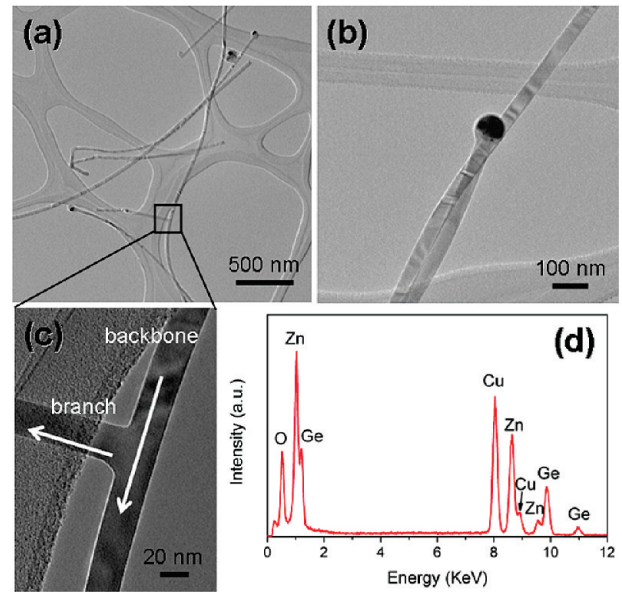

Figure 3. (a) Low magnification TEM image of the Zn_2GeO_4 nanowires. (b) High magnification TEM image of two overlapping nanowires, showing the metal catalyst particle at the growth front. (c) Enlarged view of the branched nanowire structure, where the branch grew perpendicular to the backbone nanowire. (d) EDS spectrum from individual nanowire.

indicates that the nanowires are composed of a pure Zn_2GeO_4 phase. Note that the aspect ratios of the as-synthesized Zn_2GeO_4 nanowires are significantly higher than that of the nanorods obtained by solution-involved methods before,[16,17] making them ideal candidates for further study of their electrical, optical and chemical properties.

The structures and compositions of the nanowires were further analyzed using TEM and EDS. Figure 3a is a typical low magnification TEM image of the Zn_2GeO_4 nanowires. Figure 3b is a high magnification view of two overlapping nanowires,

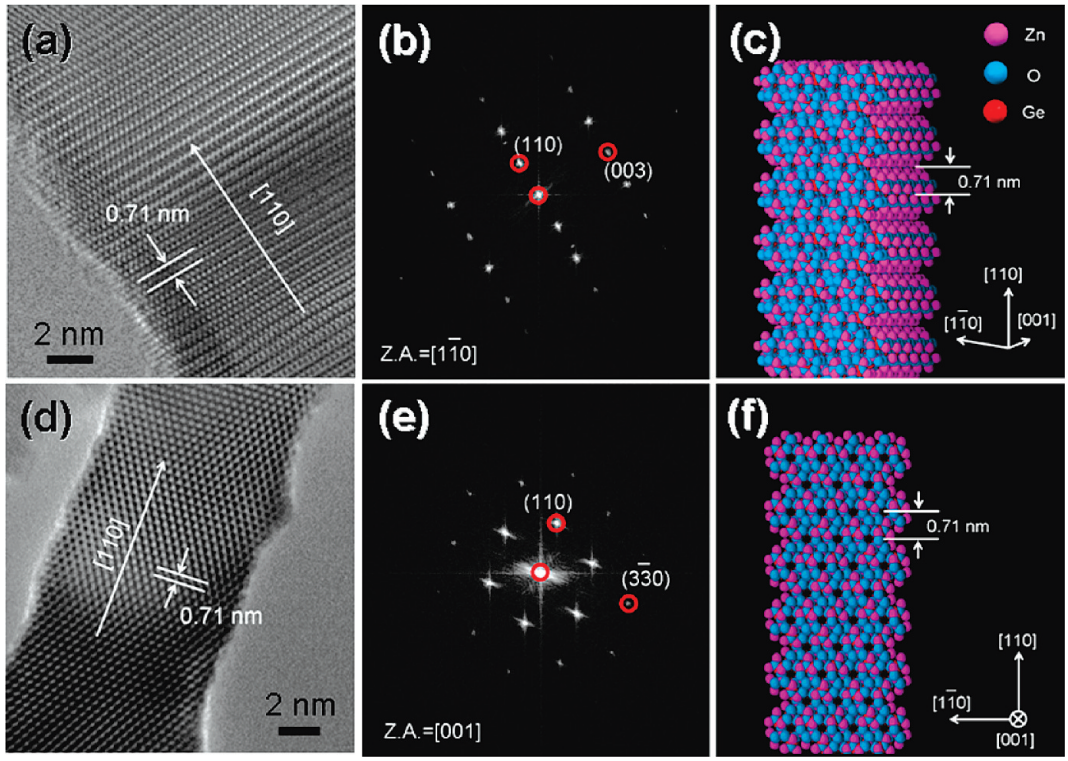

Figure 4. HRTEM images, FFT patterns, and space-filled structure models for the Zn_2GeO_4 nanowires recorded along different zone axes: (a−c) [1−10] and (d−f) [001]. For the structure models: pink, Zn; blue, O; red, Ge.

showing the metal catalyst particle at the growth front of the nanowire. The presence of the catalyst particles indicates that a VLS mechanism lies behind the nanowire growth process. Part of the as-synthesized nanowires (~5%) was found to be branched structures (Figure 3c). The branches possess preferential growth directions, which are perpendicular to the backbone nanowires (see also Figure 5). The specific orientations of the branches indicate the homoepitaxial growth (structural details are discussed below). Chemical compositions of the nanowires were characterized using EDS attached to the TEM system. EDS spectrum taken from individual nanowire is shown in Figure 3d, revealing that the nanowire is composed of Zn, Ge, and O. The atomic ratio of Zn to Ge is around 2, which is consistent with the stoichiometric value for Zn_2GeO_4. Peaks of Cu come from the Cu grid used for TEM characterization.

Detailed crystal structures of the straight Zn_2GeO_4 nanowires were characterized using HRTEM. Typical HRTEM image of the Zn_2GeO_4 nanowire recorded along [1−10] zone axis is shown in Figure 4a. Its corresponding 2D fast Fourier transforms (FFT) is shown in Figure 4b. Growth direction of the nanowire is along [110] direction of the rhombohedral Zn_2GeO_4 phase. Measured lattice spacing of 0.71 nm corresponds to the spacing between adjacent (110) planes (Figure 4a). HRTEM image and FFT pattern recorded along [001] zone axis are shown in parts d and e of Figure 4, respectively. The growth direction of the nanowire determined from FFT pattern is also along [110] direction. Space-filled structure models along the two different zone axes of [1−10] and [001] are shown in parts c and f of Figure 4, respectively. The atomic structure models are compiled along the [110] direction in order to be consistent with the experimental HRTEM observations. As shown in Figure 4c,f, the atom arrangement viewed along [1−10] zone axis is layer-like (Figure 4c); however, a close-packing-like atom arrangement can be observed if viewing from [001] zone axis (Figure 4f). Experimental observations (Figure 4a,d) show excellent agreement with the space-filled structure models. Further examinations revealed that majority of the straight nanowires grew along [110] direction, with a small number of them exhibiting ⟨113⟩ growth direction (Figure S1, Supporting Information).

Crystallographic relationships of the branched nanowires were also characterized using HRTEM in more detail. A typical TEM image (Figure 5a) shows a perpendicularly grown branch with respect to the backbone nanowire. Corresponding HRTEM images of the backbone nanowire and junction (indicated by squares in Figure 5a) are shown in parts b and c of Figure 5, respectively. The HRTEM images reveal that the branched Zn_2GeO_4 nanowires are single crystalline with no defects observed at the backbone−branch junction, in agreement with homoepitaxial growth. Growth direction of the backbone nanowire is along [110], which is the same with the straight nanowires (Figure 4). The branch grows along the [−11−3] direction, terminating with the (−11−1) top surface (Figure 5c inset); the perpendicular crystallographic relationship between the backbone nanowire and branch is consistent with the angle between these two directions for the rhombohedral Zn_2GeO_4 structure.

The effects of several growth parameters, including growth temperature, usage of Au catalyst, and ZnO/Ge molar ratio in the source materials, were also investigated. The optimum growth temperature range for ternary Zn_2GeO_4 nanowire growth according to our series of experiments at different temperature regions is 400−500 °C. For example, in the temperature region of 500−600 °C, the products are mainly composed of sponge-like impurities with some short nanorods deposited on the substrate (Figure S2, Supporting Information). In the temperature region of 400−500 °C, large quantities of long nanowires with uniform diameters were produced. XRD and EDS analyses showed that the high quality products were composed of pure Zn_2GeO_4 nanowires. There are essentially nothing deposited on the substrates at temperature regions higher than 600 °C or lower than 400 °C. Au was shown to be essential to produce high quality Zn_2GeO_4 nanowires. Without Au catalyst, the substrate was mainly covered with polycrystalline

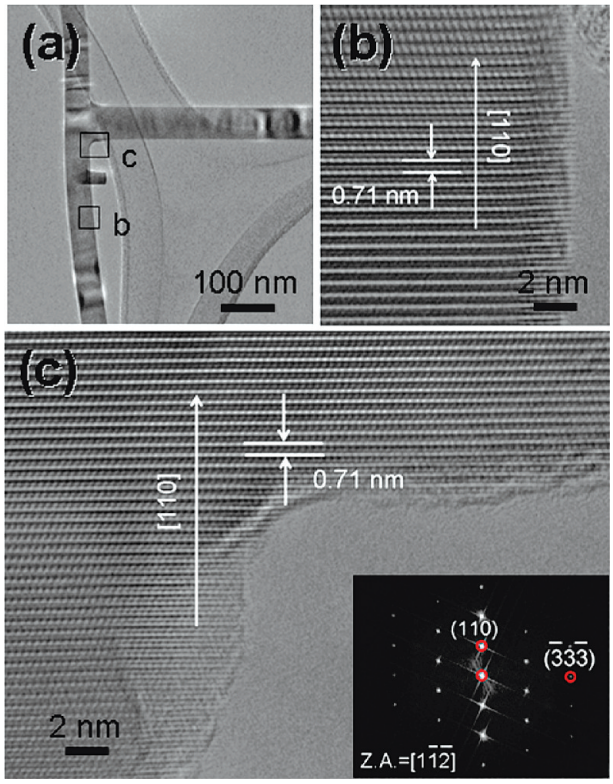

Figure 5. (a) Low magnification TEM image of a branched nanowire structure. (b,c) HRTEM images of the backbone nanowire and backbone-branch junction. The corresponding positions are indicated by squares in (a). Inset in (c) is the FFT pattern along [1−1−2] zone axis.

films and microparticles after growth (Figure S3, Supporting Information). This means that vapor−solid (VS) mechanism is not an optimum synthesis method for the Zn_2GeO_4 nanowire growth in our system. A ZnO/Ge molar ratio of 2/1 was determined to be the optimum value for the growth of high purity Zn_2GeO_4 nanowires. Excess amounts of ZnO or Ge resulted in the formation of additional ZnO or Ge phases apart from the Zn_2GeO_4 phase (Figure S4, Supporting Information). From the literature, it is well-known that ZnO and Ge nanowires can be synthesized via Au-catalyzed VLS mechanism.[1,22] However, in our case, the deposition of ternary Zn_2GeO_4 phase is attributed to the simultaneous adsorption and precipitation of Zn and Ge growth species (details are discussed below).

The Zn_2GeO_4 nanowires were synthesized via VLS mechanism, where Au serves as catalyst to direct the nanowire growth (Figure 6a). The detailed evaporation and deposition processes for the ternary and stoichiometric reactions are described as follows: Zn and Ge vapors were generated at the high temperature region (1000 °C) either through carbon-thermal reduction of ZnO or direct evaporation of Ge. The vapors would diffuse to the lower temperature region due to the concentration gradients.[23] Au nanoparticles serve as preferential adsorption sites of the vapors due to their large accommodation coefficient,[24] forming liquidus Au−Zn−Ge ternary alloy. Note that although the data of Au−Zn−Ge ternary phase diagram is lacking until now, we suggest that the catalyst particles were in liquid state during growth because the catalysts exhibit spherical shapes with smooth surfaces, which is a key indicator of the liquid state during growth.[22,25] When the Au nanoparticles reached supersaturation with Zn and Ge, precipitation at the alloy−substrate interface resulted in nanowire nucleation and growth. The relative Zn/Ge vapor concentration is controlled by the molar ratio of ZnO/Ge in the source materials, and the

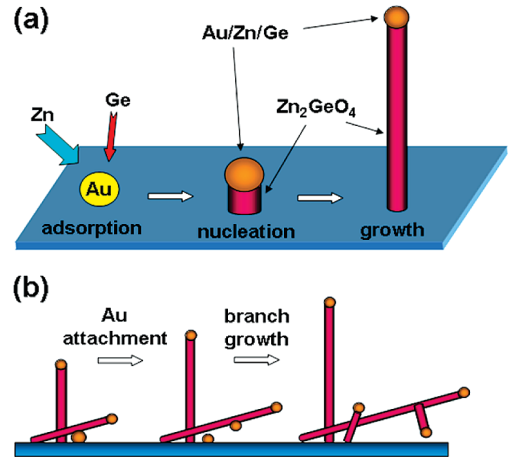

Figure 6. Growth models for the (a) straight and (b) branched Zn_2GeO_4 nanowires.

optimum value was found to be 2 (see Experimental Section). The molar ratio of ZnO/Ge in the source materials determines the relative Zn/Ge concentration in the vapor and hence in the ternary Au/Zn/Ge alloy and finally leads to the precipitation of stoichiometric Zn_2GeO_4 nanowires. Instead of the growth of Ge or ZnO nanowires, the simultaneous evaporation, adsorption, and precipitation of Ge and Zn containing species result in the formation of ternary Zn_2GeO_4 phase. It was also shown previously that the Zn_2GeO_4 phase was a thermodynamically stable phase for the ternary Zn−Ge−O system.[17] CO or mixed CO/CO_2 vapors were generated in the carbon-thermal reduction reactions and acted as the oxygen sources.[20,26] The oxygen source may also come from the residual oxygen in the furnace chamber.[8] The evaporation and deposition processes can be briefly described as:

$$\mathrm{Ge}(s) \xrightarrow{1000^\circ\mathrm{C}} \mathrm{Ge}(v) \quad (1)$$

$$\mathrm{ZnO}(s) + \mathrm{C}(s) \xrightarrow{1000^\circ\mathrm{C}} \mathrm{Zn}(v) + \mathrm{CO}(v) \quad (2)$$

$$\mathrm{Zn}(v) + \mathrm{Ge}(v) + \mathrm{CO/O_2}(v) \xrightarrow[400-500^\circ\mathrm{C}]{\mathrm{Au}} \mathrm{Zn_2GeO_4}(s) \quad (3)$$

Apart from acting as the reduction agent in eq 2, carbon also serves to maintain the Ge vapor pressure during growth. Because the formation of Ge/C compound is not thermodynamically favorable,[27] addition of carbon drastically prevents the molten Ge from agglomeration into large droplets. The high surface area of the Ge particles and hence a relatively constant Ge vapor pressure were retained.[27]

A growth model for the synthesis of branched Zn_2GeO_4 nanowires is shown in Figure 6b. Previously, several methods were employed for the synthesis of branched nanowire structures, including secondary catalyst deposition,[28,29] catalyst surface migration,[30−34] and direct condensation of catalyst from the vapor phase.[35] However, in our case, no secondary Au catalysts were deposited to direct the branch growth. Significant Au surface diffusion is also not expected due to the usage of oxide source materials and relatively abundant residual oxygen concentration, which was shown to inhibit the Au diffusion

previously.[30,31] We suggest that the Au catalysts for secondary branching come from the Au droplets on the Si substrate, which may attach to the primary nanowire surface during growth and induce branch formation.[8] The Zn_2GeO_4 nanowires on the substrate are of high density and multilayer stacking (Figure 2a). The Au droplets may attach to the nanowire surface during growth, especially for those nanowires lying at the bottom layer (nearest to the substrate surface). Consequently, the attached Au nanoparticles served as catalysts for branch growth upon continuous vapor adsorption. In contrast to the branches induced by catalysts from secondary-deposition,[28,29] the density of Zn_2GeO_4 branches is much lower (typically only one branch grown on each backbone nanowire). Also, unlike the branches induced by catalysts from surface migration,[32,34] the Zn_2GeO_4 branches showed comparable diameters with the backbone nanowire. Moreover, only ~5% of the as-synthesized nanowires were found to be branched. The low branch density, comparable diameters, and low yield of the branched products can be understood according to the growth model described above.

Previously, Zn_2GeO_4 nanorods obtained by aging Zn-containing Ge nanoparticles in water showed a dominant growth direction along [001].[17] However, in this report, the Au-catalyzed Zn_2GeO_4 nanowires mainly grow along [110] direction. This can be understood by considering the different growth mechanisms. At the nucleation stage of the Au-catalyzed VLS process, the liquid−solid interface tends to be the crystal facet with minimum surface energy,[36] resulting in a growth direction normal to the low energy surface as growth proceeds. Without mediation of Au catalyst or other surfactants, facets with higher surface energy exhibit faster growth rate according to crystal growth theory; this however results in a growth direction normal to the high energy surface. As a result, Zn_2GeO_4 nanorods[17] and nanowires (this report) synthesized without and with catalysts showed different preferential growth directions along [001] and [110], respectively. Similar effects were previously demonstrated for nanowires synthesis of various materials. For example, Si nanowires synthesized via VLS mechanism with heterogeneous metal catalysts were reported to grow along the [111] direction,[3] while nanowires synthesized via catalyst-free method were shown to grow along the [110] or [112] directions.[37]

4. Conclusions

In summary, high quality Zn_2GeO_4 nanowires were synthesized via a chemical vapor transport method using Au as metal catalysts. A majority of the as-synthesized Zn_2GeO_4 nanowires were straight, with ~5% of them being branched structures. The straight nanowires were single crystalline with a dominant growth direction along [110] direction of the rhombohedral crystal phase. Single crystal branched nanowires were also obtained through homoepitaxial growth. The branches exhibited preferential orientations that were perpendicular to the backbone nanowires. Liquidus Au droplets at the substrate surface may attach to the nanowire surface and direct the branch growth. The Au-catalyzed chemical vapor transport method for Zn_2GeO_4 nanowire synthesis may offer better control over their morphologies and structures. The novel Zn_2GeO_4 nanowires possess substantial opportunities for catalysis, optoelectronics, and display applications.

Acknowledgment. We thank P. Darmawan, M. Y. Chan, N. Singh, and J. M. Wang for their insightful discussions. We also thank S. C. Lim, S. S. Pramana, and J. Guo for their technical support.

Supporting Information Available: HRTEM and FE-SEM images of the nanowires grown under different conditions. This material is available free of charge via the Internet at http://pubs.acs.org.

References and Notes

(1) Huang, M. H.; Mao, S.; Feick, H.; Yan, H. Q.; Wu, Y. Y.; Kind, H.; Weber, E.; Russo, R.; Yang, P. D. *Science* **2001**, *292*, 1897.
(2) Dai, Z. R.; Pan, Z. W.; Wang, Z. L. *Adv. Funct. Mater.* **2003**, *13*, 9.
(3) Morales, A. M.; Lieber, C. M. *Science* **1998**, *279*, 208.
(4) Pan, Z. W.; Dai, Z. R.; Wang, Z. L. *Science* **2001**, *291*, 1947.
(5) Li, C.; Zhang, D. H.; Han, S.; Liu, X. L.; Tang, T.; Zhou, C. W. *Adv. Mater.* **2003**, *15*, 143.
(6) Choi, Y. C.; Kim, W. S.; Park, Y. S.; Lee, S. M.; Bae, D. J.; Lee, Y. H.; Park, G. S.; Choi, W. B.; Lee, N. S.; Kim, J. M. *Adv. Mater.* **2000**, *12*, 746.
(7) Kolmakov, A.; Klenov, D. O.; Lilach, Y.; Stemmer, S.; Moskovits, M. *Nano Lett.* **2005**, *5*, 667.
(8) Yan, C. Y.; Chan, M. Y.; Zhang, T.; Lee, P. S. *J. Phys. Chem. C* **2009**, *113*, 1705.
(9) Yin, Y. D.; Zhang, G. T.; Xia, Y. N. *Adv. Funct. Mater.* **2002**, *12*, 293.
(10) Pinna, N.; Willinger, M.; Weiss, K.; Urban, J.; Schlogl, R. *Nano Lett.* **2003**, *3*, 1131.
(11) Fan, H. J.; Yang, Y.; Zacharias, M. *J. Mater. Chem.* **2009**, *19*, 885.
(12) Lewis, J. S.; Holloway, P. H. *J. Electrochem. Soc.* **2000**, *147*, 3148.
(13) Liu, Z. S.; Jing, X. P.; Wang, L. X. *J. Electrochem. Soc.* **2007**, *154*, H500.
(14) Bender, J. P.; Wager, J. F.; Kissick, J.; Clark, B. L.; Keszler, D. A. *J. Lumin.* **2002**, *99*, 311.
(15) Sato, J.; Kobayashi, H.; Ikarashi, K.; Saito, N.; Nishiyama, H.; Inoue, Y. *J. Phys. Chem. B* **2004**, *108*, 4369.
(16) Huang, J. H.; Wang, X. C.; Hou, Y. D.; Chen, X. F.; Wu, L.; Fu, X. Z. *Environ. Sci. Technol.* **2008**, *42*, 7387.
(17) Tsai, M. Y.; Yu, C. Y.; Wang, C. C.; Perng, T. P. *Cryst. Growth Des.* **2008**, *8*, 2264.
(18) Jung, Y.; Lee, S. H.; Ko, D. K.; Agarwal, R. *J. Am. Chem. Soc.* **2006**, *128*, 14026.
(19) Peng, H. L.; Schoen, D. T.; Meister, S.; Zhang, X. F.; Cui, Y. *J. Am. Chem. Soc.* **2007**, *129*, 34.
(20) Wang, Z. L. *Mater. Sci. Eng. R* **2009**, *64*, 33.
(21) Geng, C. Y.; Jiang, Y.; Yao, Y.; Meng, X. M.; Zapien, J. A.; Lee, C. S.; Lifshitz, Y.; Lee, S. T. *Adv. Funct. Mater.* **2004**, *14*, 589.
(22) Kodambaka, S.; Tersoff, J.; Reuter, M. C.; Ross, F. M. *Science* **2007**, *316*, 729.
(23) Mensah, S. L.; Kayastha, V. K.; Yap, Y. K. *J. Phys. Chem. C* **2007**, *111*, 16092.
(24) Wanger, R. S.; Ellis, W. C. *Appl. Phys. Lett.* **1964**, *4*, 89.
(25) Schmidt, V.; Gosele, U. *Science* **2007**, *316*, 698.
(26) Yang, P. D.; Yan, H. Q.; Mao, S.; Russo, R.; Johnson, J.; Saykally, R.; Morris, N.; Pham, J.; He, R. R.; Choi, H. J. *Adv. Funct. Mater.* **2002**, *12*, 323.
(27) Wu, J.; Punchaipetch, P.; Wallace, R. M.; Coffer, J. L. *Adv. Mater.* **2004**, *16*, 1444.
(28) Dick, K. A.; Deppert, K.; Larsson, M. W.; Martensson, T.; Seifert, W.; Wallenberg, L. R.; Samuelson, L. *Nat. Mater.* **2004**, *3*, 380.
(29) Wang, D.; Qian, F.; Yang, C.; Zhong, Z. H.; Lieber, C. M. *Nano Lett.* **2004**, *4*, 871.
(30) Hannon, J. B.; Kodambaka, S.; Ross, F. M.; Tromp, R. M. *Nature* **2006**, *440*, 69.
(31) Kodambaka, S.; Hannon, J. B.; Tromp, R. M.; Ross, F. M. *Nano Lett.* **2006**, *6*, 1292.
(32) Doerk, G. S.; Ferralis, N.; Carraro, C.; Maboudian, R. *J. Mater. Chem.* **2008**, *18*, 5376.
(33) Denhertog, M. I.; Rouviere, J. L.; Dhalluin, F.; Desre, P. J.; Gentile, P.; Ferret, P.; Oehler, F.; Baron, T. *Nano Lett.* **2008**, *8*, 1544.
(34) Kawashima, T.; Mizutani, T.; Nakagawa, T.; Torii, H.; Saitoh, T.; Komori, K.; Fujii, M. *Nano Lett.* **2008**, *8*, 362.
(35) Gao, P. X.; Wang, Z. L. *J. Phys. Chem. B* **2002**, *106*, 12653.
(36) Wu, Y.; Cui, Y.; Huynh, L.; Barrelet, C. J.; Bell, D. C.; Lieber, C. M. *Nano Lett.* **2004**, *4*, 433.
(37) Kim, B. S.; Koo, T. W.; Lee, J. H.; Kim, D. S.; Jung, Y. C.; Hwang, S. W.; Choi, B. L.; Lee, E. K.; Kim, J. M.; Whang, D. *Nano Lett.* **2009**, *9*, 864.

JP9050879